



HAL
open science

Asynchronous global–local non-invasive coupling for nonlinear monotone patches: Application to plasticity problems

Ahmed El Kerim, Pierre Gosselet, Frédéric Magoulès

► **To cite this version:**

Ahmed El Kerim, Pierre Gosselet, Frédéric Magoulès. Asynchronous global–local non-invasive coupling for nonlinear monotone patches: Application to plasticity problems. *Computer Methods in Applied Mechanics and Engineering*, 2024, 430, pp.117166. 10.1016/j.cma.2024.117166 . hal-04667972

HAL Id: hal-04667972

<https://hal.science/hal-04667972v1>

Submitted on 5 Aug 2024

HAL is a multi-disciplinary open access archive for the deposit and dissemination of scientific research documents, whether they are published or not. The documents may come from teaching and research institutions in France or abroad, or from public or private research centers.

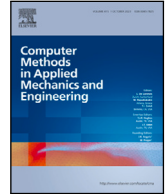
L'archive ouverte pluridisciplinaire **HAL**, est destinée au dépôt et à la diffusion de documents scientifiques de niveau recherche, publiés ou non, émanant des établissements d'enseignement et de recherche français ou étrangers, des laboratoires publics ou privés.



Distributed under a Creative Commons Attribution - NonCommercial - NoDerivatives 4.0 International License

Contents lists available at [ScienceDirect](https://www.sciencedirect.com)

Comput. Methods Appl. Mech. Engrg.

journal homepage: www.elsevier.com/locate/cma

Asynchronous global–local non-invasive coupling for nonlinear monotone patches: Application to plasticity problems

Ahmed El Kerim ^{a,c}, Pierre Gosselet ^b, Frédéric Magoulès ^{c,d,*}

^a Université Paris-Saclay, CentraleSupélec, ENS Paris-Saclay, CNRS, LMPS, Gif-sur-Yvette, 91190, France

^b Univ. Lille, CNRS, Centrale Lille, UMR 9013 - LaMcube, Lille, F-59000, France

^c Université Paris-Saclay, CentraleSupélec, MICS, Gif-sur-Yvette, 91190, France

^d Faculty of Engineering and Information Technology, University of Pécs, Pécs, H-7622, Hungary

ARTICLE INFO

Keywords:

Asynchronous global–local coupling
Asynchronous methods
Iterative methods
Nonlinear monotone patches
Non-invasive coupling
Plasticity problem

ABSTRACT

This article presents the asynchronous global–local non-invasive coupling in the case of nonlinear monotone patches as encountered when inserting elastoplastic components in a global linear elastic model. The convergence of the method is theoretically established in a general framework using the paracontractions technique and illustrated in academic examples with a weak scalability study considering the case of balanced and unbalanced patches.

1. Introduction

The global–local coupling technique is a computational method that aims at simplifying the study of local alterations inside the finite element model of a structure. Compared to the classical submodeling approach, it is a two-way method in the sense that all interactions (global model \leftrightarrow local patches) are accounted for. This method is particularly precious for industrialists since it easily adapts to their design workflow, starting from a simplified model of a structure and progressively introducing details. The global–local coupling makes it possible to compute the exact effects of the details without requiring to modify the model which is a time-consuming and hard to automate stage. Moreover, due to the classical quantities to be exchanged between the global and local models (displacement and traction), the coupling is non-invasive, as all computations can be carried out on industrial (closed) software. The method can even be employed to associated commercial and research software, bringing new functionalities inside legacy code, see [1] for an implementation using Abaqus co-simulation engine.

The main requirement to employ the global–local coupling method is the well-posedness of local Dirichlet problems, which is often encountered in mechanical problems. It opens the path to its application in many contexts like, among others, local plasticity [2], crack propagation in a sound model [3], explicit dynamics [4], plate/three-dimensional modeling of assemblies [5], uncertainty quantification [6], computation of elastoviscoplastic models with mesh refinement [7], debonding of composite panels [8], brittle fracture with phase-field modeling [9,10].

Despite its strong link with domain decomposition methods (see [11] for the interpretation as an alternate Robin–Dirichlet method and [12] as a primal domain decomposition method), the global–local coupling cannot pretend to high performance computing. In comparison with other nonlinear domain decomposition methods [13,14], it is much less parallel due to the central role played by the global problem. When considered as a modeling assistant which helps the designer introduce details in a global

* Corresponding author.

E-mail address: frederic.magoules@hotmail.com (F. Magoulès).

<https://doi.org/10.1016/j.cma.2024.117166>

Received 1 February 2024; Received in revised form 24 May 2024; Accepted 15 June 2024

Available online 14 July 2024

0045-7825/© 2024 The Author(s). Published by Elsevier B.V. This is an open access article under the CC BY-NC-ND license (<http://creativecommons.org/licenses/by-nc-nd/4.0/>).

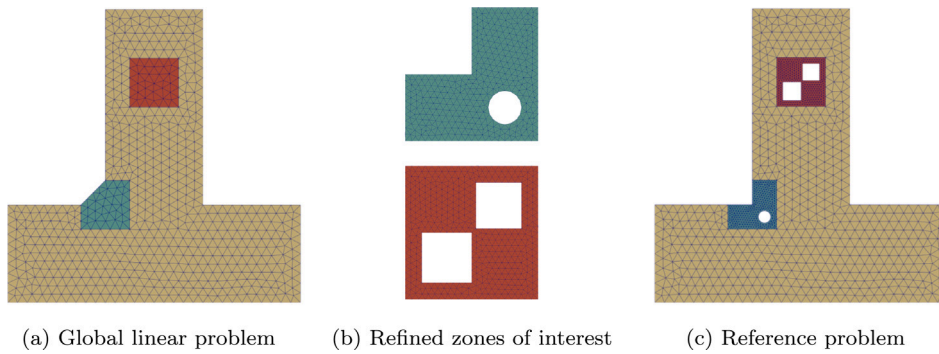


Fig. 1. Models and subdomains for the Global/Local coupling.

structure, scalability does not appear to be an important feature. Handling efficiently few hundreds of patches seems to be an objective in agreement with industrialists' practice.

In order to unleash as much computational power as possible, asynchronous parallel computing has emerged as a promising approach. It allows each subdomain to work independently, asynchronously updating its solution and exchanging information with neighboring subdomains when possible. This property can be particularly precious when patches are poorly-balanced because nonlinearity is non-evenly distributed. Several works have focused on classical alternating Schwarz methods with overlap, providing theoretical convergence proofs and numerical illustrations [15–18]. In [19], an asynchronous version of the weighted additive Schwarz method is investigated, demonstrating its convergence and significant improvement compared to the synchronous version. The application of the asynchronous alternating Schwarz method to a large structural mechanics problem using the supercomputer Grid5000 is presented in [20]. In [21], an asynchronous additive Schwarz method is theoretically and numerically investigated to solve nonlinear problems with a finite difference scheme. The rate of convergence of asynchronous domain decomposition methods is studied in the context of convex optimization in [22]. Recently, [23] introduces a novel scalable asynchronous two-level Schwarz method.

Regarding non-overlapping methods, which are particularly suitable for mechanical problems, recent works achieved interesting results with asynchronous approach. In [24], a convergence proof of the classical substructuring method for the three-dimensional Poisson problem is provided. In [25] a Gauss–Seidel scheme is proposed to alternate between the resolution on the interface and in the subdomains. Furthermore, [26] improves the method by introducing a coarse space correction that enhances its scalability. Various applications of the asynchronous optimized Schwarz method [27] are discussed in [28–30]. Other studies have explored the convergence of asynchronous domain decomposition methods, such as primal Schur domain decomposition [31] and asynchronous multigrid methods [32].

In [12], an asynchronous version of the non-invasive global–local coupling method was presented for linear problems in structural mechanics. A proof of convergence was provided by analyzing the spectrum of an operator corresponding to repeated iterations. This paper aims at extending asynchronous iteration to a larger class of mechanical problems. Our approach relies on certain algebraic structures and energy bounds which correspond to having a linear global model and continuous monotone patches. This framework encompasses elasto(visco)plastic mechanical models with positive hardening. Even if this may seem a restricted domain compared to the many current applications of the global-coupling, it in fact corresponds to the hypothesis of [6] where the most advanced proofs were given for the synchronous global–local iteration. Moreover, elastoviscoplastic problems correspond to a large class of industrial studies where the objective is to compute the evolution of the structure before damage or fracture threaten its lifespan. Elastoviscoplasticity requires sophisticated numerical methods to be correctly handled, like Newton–Raphson incremental solver coupled with radial mapping [33,34]. Due to the (positive) hardening, plasticity is often localized in zones of stress concentration, and the size of those zones grows smoothly with the intensity of the load. It is thus a very natural approach to start from a global linear elastic model of a structure and try to apply the nonlinear behavior only in the zones of interest where a certain elastic criterion was met, like the value of the Mises stress being close to the elastic limit.

The paper is organized as follows: Section 2 introduces to the global–local coupling method. Section 3 presents the asynchronous framework and provides convergence proofs under reasonable assumptions. Section 4 illustrates the performance on academic examples, including a weak scalability assessment.

2. Derivation of synchronous non-invasive Global/Local coupling

This section aims at providing the fundamental concepts necessary to comprehend and analyze the Global/Local coupling method applied to monotone patches with asynchronous iteration. For improved clarity, we directly consider the finite element discretization of the problem, although the same analysis could be applied to the variational formulation. We use an elastoplastic mechanical problem as an illustration, however the method can be applied to the general case of monotone elliptic problems. For simplicity, the presentation follows the basic outline of [12] and introduces novelty where needed.

The classical scenario is illustrated on Fig. 1. A **linear** elastic Global coarse model is used to describe a large structure. After the initial computation, $N > 0$ zones of interest $\Omega^{s,G}$ ($N \geq s > 0$) are selected because some criterion has been exceeded or because it was known from the beginning that some details were missing in the Global model. In our illustration, geometrical details, **elastoplastic** behavior and adapted meshes are introduced in the Local modeling of the zones of interest $\Omega^{s,F}$. Material heterogeneity could also have been introduced. Local computations are run in parallel on the patches using the Global solution as Dirichlet boundary condition (for $s > 0$, the interior of the Local and Global subdomains may differ, but their interface Γ^s must be the same $\Gamma^s = \Omega \cap \partial\Omega^{s,G} = \Omega \cap \partial\Omega^{s,F}$). For now, only one load increment is considered, more complex load sequences, which play an important role in history-dependent problems, will be studied in Section 3.5.

After these initial computations which corresponds to the submodeling technique, there exists lack of balance of the traction between the Global zone not covered by patches, denoted by $\Omega^0 = \Omega^G \setminus (\bigcup_{s>0} \Omega^{s,F})$ and the Local models. Such a stress gap would not exist in the Reference computation where the Local zones of interest would have directly inserted in the computational model, Fig. 1(c).

The Global/Local coupling is a simple iterative technique (a Richardson iteration for its simpler version) aiming at obtaining the Reference solution from computations carried on the Global and Local models with minimal intervention on the models and software. The main interest of the coupling is to avoid the creation of the Reference model which is often cumbersome operation, hard to automate and needing human intervention anytime an extra modification is applied.

2.1. Global problem

The global model (index G) is a representation of the whole structure assumed to be sufficiently well-designed to correctly grasp the stress flows in the structure. For instance one can think of a homogenized model of a heterogeneous microstructure, or a shell model for a slender structure. To fit with our current theoretical proof, we need to assume that the global problem is linear, issued from the discretization of a symmetric continuous coercive bilinear form. Note that in practice nonlinear global models have already been successfully used [3,7].

The global model is corrected by an extra load \mathbf{p}_F of nodal fluxes applied on the interface $\Gamma = \bigcup_{s=0}^N \Gamma^s$. To position the interface in the Global domain we introduce the boolean trace operator $\mathbf{T}^G : \Omega^G \rightarrow \Gamma$, so that $\mathbf{u}_F^G = \mathbf{T}^G \mathbf{u}^G$, its transpose is the extension-by-0 operator.

The discrete Global problem can be written as:

$$\left\{ \begin{array}{l} \text{For given } \mathbf{p}_F \text{ on } \Gamma, \text{ find } \mathbf{u}^G \text{ in } \Omega^G, \text{ such that} \\ \mathbf{K}^G \mathbf{u}^G = \mathbf{f}^G + \mathbf{T}^{G^T} \mathbf{p}_F \end{array} \right. \quad (1)$$

where one can recognize the symmetric definite positive stiffness matrix \mathbf{K}^G , the vector of generalized loads \mathbf{f}^G , the vector of unknowns \mathbf{u}^G . In general the initial guess for \mathbf{p}_F is zero.

2.2. Local problems

Let $\mathbf{A}^s : \Gamma^s \rightarrow \Gamma^G$ be the extension-by-zero operator (transpose of the restriction operator), and $\mathbf{T}^{s,F} : \Omega^{s,F} \rightarrow \Gamma^s$ be the local trace operator. In order to handle potentially non-conforming discretizations between the global and fine models, we introduce the global-to-fine interpolation operator \mathbf{J}^s . Note that more involved transfer techniques are possible, e.g. mortar methods [3].

The discrete fine problems correspond to solving independent Dirichlet problems on the patches with the boundary condition inherited from the global problem \mathbf{u}^G :

$$\left\{ \begin{array}{l} \forall s > 0, \text{ find } \mathbf{u}^{s,F} \text{ in } \Omega^{s,F} \text{ and } \lambda^{s,F} \text{ on } \Gamma^s \text{ such that} \\ - \mathbf{f}_{int}^{s,F}(\mathbf{u}^{s,F}) = \mathbf{f}^{s,F} + \mathbf{T}^{s,F^T} \lambda^{s,F} \\ \mathbf{T}^{s,F} \mathbf{u}^{s,F} = \mathbf{J}^s \mathbf{A}^{s^T} \mathbf{u}_F^G, \end{array} \right. \quad (2)$$

where $\mathbf{f}_{int}^{s,F}$ is the vector of internal forces, which corresponds to the work of the stress field in the finite element strain shape functions. $\lambda^{s,F}$ is the vector of nodal reactions associated with the interface Dirichlet condition.

Problem (2) is nonlinear, it requires an adapted iterative solver, in general a Newton–Raphson method. In the case of plasticity, solving (2) also involves updating internal variables (plastic strain, hardening) at the Gauss points, often using a θ -method. In this study, we assume that the error from the nonlinear solver is negligible with respect to the coupling error. The gains to be expected from the use of an inexact solver will be the subject of a forthcoming study.

We need to introduce the piece Ω^0 of the global domain that may not be covered by the fine patches $\Omega^0 = \Omega \setminus (\bigcup_{s>0} \overline{\Omega^s})$. Note that possibly Ω^0 can be empty. In the literature, Ω^0 was sometime referred to as the complement domain. It can also be viewed as the subdomain where the fine and global models coincide. Ω^0 is useful in order to post-process λ^0 , the global reaction from its side of the interface:

$$\text{Given } \mathbf{u}^G, \quad \lambda^0 = \mathbf{T}^{0^T} (\mathbf{K}^0 \mathbf{u}_{|\Omega^0}^G - \mathbf{f}^0). \quad (3)$$

Note that this computation can be conducted only on a halo around the interface, or using integration features of certain finite element software. To gather notations later, we introduce $\mathbf{J}^0 = \mathbf{I}_\Gamma$.

2.3. Residual and iterations

The residual \mathbf{r} can be defined as:

$$\mathbf{r} = - \left(\mathbf{A}^0 \lambda^0 + \sum_{s>0} \mathbf{A}^s \mathbf{J}^{sT} \lambda^{s,F} \right). \quad (4)$$

The residual corresponds to the lack of balance between patches at the interface. It measures how unfit the common Dirichlet condition \mathbf{u}^G was. Small \mathbf{r} means that the displacement \mathbf{u}^G is a good guess of the actual displacement of the reference problem constituted by the assembly of the complement domain Ω^0 and the fine models $(\Omega^{s,F})_{s>0}$.

We can then consider a simple Richardson iteration in order to improve \mathbf{u}^G , leading to the corrected global problem and the following sequence of computations:

- (0) Starting from $\mathbf{p}_\Gamma = 0$,
- (1) Compute the corrected global problem: $\mathbf{K}^G \mathbf{u}^G = \mathbf{f}^G + \mathbf{T}^{GT} \mathbf{p}_\Gamma$,
- (2) Post-process the global reaction λ^0 as in eq. (4),
- (3) Solve the fine Dirichlet problems (2), compute the reactions $(\lambda^{s,F})_{s>0}$ (5)
- (4) Assemble the residual $\mathbf{r} = - \left(\mathbf{A}^0 \lambda^0 + \sum_{s>0} \mathbf{A}^s \mathbf{J}^{sT} \lambda^{s,F} \right)$,
- (5) Update the corrective load $\mathbf{p}_\Gamma \leftarrow \mathbf{p}_\Gamma + \omega \mathbf{r}$, go to (1).

Here, $\omega > 0$ is a relaxation parameter of the method. Aitken's Δ^2 dynamic relaxation appears to be a very efficient technique to tune it automatically.

2.4. Discussion

The Global problem (1) is a well-posed linear elastic mechanical problem, which implies the possibility to process the global reaction (4). For the global–local coupling iteration to be well-defined, it is necessary for the Local nonlinear problems with Dirichlet condition (2) to be well-posed so that the reaction can be processed on the interface. This vague framework made it possible to use the method successfully in many different cases including fracture [3,9,35] (using phase-field or XFEM approaches) or delamination [36]. Even if the method often converges to a solution where all mechanical equations are satisfied, it is not clear, due to the softening nature of such problems which allows for multiple solutions, that the use of the global/local coupling does not drive the solution to a specific branch that would be hard to follow considering the reference problem. Same issue appears in friction contact problems [5] where uniqueness is not granted. This is even clearer in the case of multiple patches where bad guess of \mathbf{p}_Γ might lead to the ruin of one patch and the irremediable choice of a solution path.

In fact, a certain stability is required for the local problems in order to make sure that the reference problem has a unique solution, towards which the global–local iteration converges. In [6], it was proved that assuming monotone and continuous behavior in the fine patches (see later for more detail and refer to [6] for comprehensive analysis including stochastic effects), there exist a non-empty interval of the form $(0, \omega_0)$ where the (synchronous) iteration converges to the reference solution. Nonlinear problems characterized by a monotone operator form an important class of well-posed mathematical problems where the solution can be reached by fixed-point iterations, even asynchronous [37]. Mechanically speaking, monotone models can be obtained for elasto(visco)plastic materials in small strains with positive hardening [38, lemma 2], which is linked to the Drucker stability property [39] and to Hill's maximal plastic work principle.

The proof in [6] was carried out in the continuous setting with a single patch, which is equivalent to the synchronous iteration for a family of non-connected patches, and then applied to the discretized system. We place our study in the same framework, and our objective is to extend the convergence proof to multiple patches with asynchronous iteration. In order to simplify our presentation and avoid some cumbersome functional analysis issues, in particular for the handling of contiguous patches, our analysis is directly applied to the discrete system, nevertheless the properties that underlie the convergence are the same in the continuous and the discrete settings. In order to even further simplify the presentation, the starting point of our analysis is the condensed system described in next subsection.

2.5. Condensation

Because all manipulated data are associated with mechanical problems in balance, and thanks to the well-posedness of the local Dirichlet problems induced by the chosen hypotheses, the convergence is driven by the interface, and it is convenient to formally eliminate internal degrees of freedom (index i) and to condense all problems at the interface (index Γ).

2.5.1. Global problem

The condensation of linear operators is a classical operation. It leads to the introduction of the Schur complement matrix \mathbf{S}^G and the condensed right-hand side \mathbf{b}^G :

$$\mathbf{K}^G \mathbf{u}^G = \mathbf{f}^G + \mathbf{T}^{GT} \mathbf{p}_F \Leftrightarrow \begin{cases} \mathbf{u}_i^G = \mathbf{K}_{ii}^{G^{-1}} (\mathbf{f}_i^G - \mathbf{K}_{iF} \mathbf{u}_F^G) \\ \mathbf{S}^G \mathbf{u}_F^G = \mathbf{b}^G + \mathbf{p}_F \end{cases} \quad (6)$$

where $\mathbf{S}^G = \mathbf{K}_{FF}^G - \mathbf{K}_{Fi}^G \mathbf{K}_{ii}^{G^{-1}} \mathbf{K}_{iF}^G$ and $\mathbf{b}^G = \mathbf{f}_F^G - \mathbf{K}_{Fi}^G \mathbf{K}_{ii}^{G^{-1}} \mathbf{f}_i^G$

The Schur complement inherits the symmetric definite positive nature of \mathbf{K}^G . Note that the global Schur complement is the sum of subdomains' contributions:

$$\mathbf{S}^G = \sum_{s=0}^N \mathbf{A}^s \mathbf{S}^{s,G} \mathbf{A}^{sT}, \quad \text{with } \mathbf{S}^{s,G} = \mathbf{K}_{FF}^{s,G} - \mathbf{K}_{Fi}^{s,G} \mathbf{K}_{ii}^{s,G^{-1}} \mathbf{K}_{iF}^{s,G}, \quad (7)$$

and that the local Schur complements may be semi-definite in the absence of Dirichlet conditions.

2.5.2. Euclidean structures induced by the Global model

The global model allows us to introduce the following norms which are equivalent to the canonical ones (even in the continuous setting):

Local stiffness seminorm for local displacement:

$$\forall s, \forall \mathbf{u}_F^{s,G}, \left| \mathbf{u}_F^{s,G} \right|_{\mathbf{S}^{s,G}}^2 := \mathbf{u}_F^{s,GT} \mathbf{S}^{s,G} \mathbf{u}_F^{s,G}, \quad (8)$$

Global compliance inner product and norm for global reactions:

$$\forall (\mathbf{a}_F^G, \mathbf{b}_F^G), \quad \begin{cases} \langle \mathbf{a}_F^G, \mathbf{b}_F^G \rangle_G := \mathbf{a}_F^{GT} \mathbf{S}^{G^{-1}} \mathbf{b}_F^G, \\ \|\mathbf{a}_F^G\|_G := \langle \mathbf{a}_F^G, \mathbf{a}_F^G \rangle_G^{1/2}. \end{cases} \quad (9)$$

2.5.3. Patches

We introduce the local Dirichlet-to-Neumann (DtN) maps. The nodal reactions ($\lambda^{s,F}$) on the subdomains' interface are written as a function of the imposed Dirichlet condition $\mathbf{u}_F^{s,F}$:

$$\lambda^{s,F} = \mathbf{s}^{s,F}(\mathbf{u}_F^{s,F}; \mathbf{f}^{s,F}) \text{ means } \begin{cases} \exists \mathbf{v}^{s,F} \text{ such that } \begin{cases} \mathbf{T}^{s,F} \mathbf{v}^{s,F} = \mathbf{u}_F^{s,F} \\ (\mathbf{f}_{int}^s(\mathbf{v}^{s,F}) + \mathbf{f}^{s,F})_i = 0 \end{cases} \\ \lambda^{s,F} := -(\mathbf{f}_{int}^{s,F}(\mathbf{v}^{s,F}) + \mathbf{f}^{s,F})_F \end{cases} \quad (10)$$

For linear subdomains, in particular Ω^0 if it exists, the Dirichlet-to-Neumann operators takes the form of an affine operator. For instance, we have:

$$\lambda^0 = \mathbf{s}^0(\mathbf{u}_F^0; \mathbf{f}^0) = \mathbf{S}^0 \mathbf{u}_F^0 - \mathbf{b}^0 = \mathbf{T}^0 (\mathbf{K}^0 \mathbf{u}_F^0 - \mathbf{f}^0) \quad (11)$$

2.5.4. Global-Local iteration in term of condensed operator

The sequence of operations of (5) can be rewritten as:

$$\mathbf{p}_F \leftarrow \mathbf{p}_F - \omega \left(\sum_{s \geq 0} \mathbf{A}^s \mathbf{J}^{sT} \mathbf{s}^{s,F} \left(\mathbf{J}^s \mathbf{A}^{sT} \mathbf{S}^{G^{-1}} (\mathbf{b}^G + \mathbf{p}_F); \mathbf{f}^{s,F} \right) \right) \quad (12)$$

If the iterations converge, the limit $\hat{\mathbf{p}}_F$ solves the coupling problem (null residual in (4)):

$$\sum_{s \geq 0} \mathbf{A}^s \mathbf{J}^{sT} \mathbf{s}^{s,F} \left(\mathbf{J}^s \mathbf{A}^{sT} \mathbf{S}^{G^{-1}} (\mathbf{b}^G + \hat{\mathbf{p}}_F); \mathbf{f}^{s,F} \right) = 0 \quad (13)$$

2.5.5. Hypotheses

The monotonicity and continuity hypotheses are initially formulated on the partial differential equation (PDE) to be solved. These hypotheses have direct consequences on the Dirichlet-to-Neumann maps. For simplicity, our starting point are the inequalities satisfied by the DtN maps. The link with the original PDE is briefly explained in [Appendix A](#) and the reader is referred to [6] for a complete presentation.

Strong monotonicity property $\forall s > 0, \exists \gamma^s > 0$, such that $\forall (\mathbf{u}_F^{s,G}, \mathbf{v}_F^{s,G})$:

$$\left(\mathbf{s}^{s,F}(\mathbf{J}^s \mathbf{u}_F^{s,G}; \mathbf{f}^{s,F}) - \mathbf{s}^{s,F}(\mathbf{J}^s \mathbf{v}_F^{s,G}; \mathbf{f}^{s,F}) \right)^T \mathbf{J}^s (\mathbf{u}_F^{s,G} - \mathbf{v}_F^{s,G}) \geq \gamma^s \left| \mathbf{u}_F^{s,G} - \mathbf{v}_F^{s,G} \right|_{\mathbf{S}^{s,G}}^2. \quad (14)$$

Continuity property $\forall s > 0, \exists M^s > 0$ such that $\forall(\mathbf{u}_F^{s,G}, \mathbf{v}_F^{s,G})$:

$$\left\| \mathbf{A}^s \mathbf{J}^{s,T} \left(\mathbf{s}^{s,F} (\mathbf{J}^s \mathbf{u}_F^{s,G}) - \mathbf{s}^{s,F} (\mathbf{J}^s \mathbf{v}_F^{s,G}) \right) \right\|_G^2 \leq M^s \left| \mathbf{u}_F^{s,G} - \mathbf{v}_F^{s,G} \right|_{\mathbf{S}^{s,G}}^2. \quad (15)$$

Note that equivalent inequalities exist at the continuous level between Steklov–Poincaré operators (and the (semi)norms they define on appropriate Hilbert spaces). This means that the constants (γ^s, M^s) depend on the geometry, the material and the meshes, but they are not the result of the invocation of the finite dimension of the discrete problem.

Remark 1 (Case of Linear Fine Patches). For linear patches, γ^s and M^s are extreme generalized eigenvalues:

$$\begin{aligned} \gamma^s &= \min\{\lambda > 0, \det(\mathbf{J}^{s,T} \mathbf{S}^{s,F} \mathbf{J}^s - \lambda \mathbf{S}^{s,G}) = 0\} \\ M^s &= \max\{\lambda, \det(\mathbf{J}^{s,T} \mathbf{S}^{s,F} \mathbf{J}^s \mathbf{A}^s \mathbf{S}^{G-1} \mathbf{A}^s \mathbf{J}^{s,T} \mathbf{S}^{s,F} \mathbf{J}^s - \lambda \mathbf{S}^{s,G}) = 0\} \end{aligned} \quad (16)$$

3. Asynchronous global local non invasive coupling

In this section, the asynchronous version of the global–local coupling is presented, then we prove that there exist a non-empty interval for the relaxation parameter that ensures convergence, and even monotone decrease of the error in some cases.

3.1. Asynchronous algorithm

The synchronous algorithm was given in Eq. (5), in this section, we discuss its asynchronous version. The asynchronous algorithm is based on the idea that the global problem is updated as soon as new data is obtained from any of the local problems. Otherwise, it waits without performing any calculations. Similarly, the fine models in the patches can launch a computation as soon as they access new information from the global problem.

Algorithm 1: Asynchronous Global–Local Coupling

Initialization Rank 0: $\mathbf{p}_F = 0$

Windows creation. Rank 0: $[\dots \mathbf{q}^s \dots] = 0$, Rank $s > 0$: $\mathbf{u}^{s,G}$

while $\|\mathbf{r}\|$ is too large **do**

On rank 0 (Global domain), with at least one new \mathbf{q}^s ($s > 0$)

 Global computes residual $\mathbf{r} = -\sum_s \mathbf{A}^s \mathbf{q}^s$

 Global updates $\mathbf{p}_F = \mathbf{p}_F + \omega \mathbf{r}$

 Global solve system (6), $\mathbf{u}_F^G = \mathbf{S}^{G-1} (\mathbf{p}_F + \mathbf{b}^G)$

 if Ω^0 exists **then**

 Post-processing: $\mathbf{q}^0 := \lambda^0 = \mathbf{S}^0 \mathbf{u}_F^{0,G} - \mathbf{b}^{0,G}$

end

$\forall s > 0$ Global puts $\mathbf{u}^{s,G} := \mathbf{A}^{s,T} \mathbf{u}_F^G$ in the Local window

On rank $s > 0$ (Local patch) with new $\mathbf{u}^{s,G}$

 Local solves (2), $\lambda^{s,F} = \mathbf{s}^{s,F} (\mathbf{J}^s \mathbf{A}^{s,T} \mathbf{u}_F^G; \mathbf{f}^{s,F})$

 Local puts $\mathbf{q}^s := \mathbf{J}^{s,T} \lambda^{s,F}$ in the Global window.

end

Algorithm 1 presents the asynchronous version of the global–local coupling algorithm, using MPI-RDMA passive synchronization vocabulary, as presented in [12,23,30].

In this asynchronous algorithm, Rank 0 serves as the central processor that coordinates the communication and updates between the global and local components. Whenever Rank 0 detects new information from any of the patches (new $\mathbf{q}^s = \mathbf{J}^{s,T} \lambda^{s,F}$), it performs the resolution of the global system. Similarly, when a patch detects new information from the global problem (new $\mathbf{u}^{s,G} = \mathbf{A}^{s,T} \mathbf{u}_F^G$), it updates its local solution. The algorithm continues until the convergence criterion is met.

The asynchronous algorithm allows for overlapping computation and communication, leading to potentially improved efficiency in parallel environments.

3.2. Convergence of the asynchronous iteration

As presented in the introduction, several techniques exist to study the convergence of an asynchronous method. One particular difficulty in our case is the absence of the discrete maximal principle, so that the matrices do not possess the favorable M-property [40], and the objective to remain non-invasive makes it impossible to recover such a property by invasive manipulations.

A recent study [41] proved the convergence of the asynchronous Richardson iterations for linear problems with a delay bounded by 2. To generalize that study and go to the case with larger delay, the paracontraction concept introduced in [42] is used. The idea is to formulate the method as a succession of contractive operators (for a well-chosen relaxation) sharing a common fixed point. We can find other applications of this approach for linear and nonlinear problems in [43–45].

3.2.1. Paracontractions

Let (T_m) be a finite family of paracontractions with a common fixed point \hat{x} in some Hilbert space E . In other words:

- $\forall x \in E, \|T_m(x) - \hat{x}\| < \|x - \hat{x}\|$ or $T_m(x) = x$,
- $\forall m, T_m(\hat{x}) = \hat{x}$.

Then a sequence of the form:

$$x_{j+1} = T_{m(j)}(x_j) \tag{17}$$

converges to \hat{x} , assuming that all the paracontractions (T_m) are sufficiently frequently activated [42].

3.2.2. Asynchronous formulation

Before studying the convergence of the asynchronous model, a rewriting of the problem is introduced, considering the delays affecting the patches.

Referring to Algorithm 1, during the step from Iteration j to $j + 1$, it is considered that some patches provide new pieces of information in order to evaluate the residual, anyhow these pieces of information may be related to old configurations $\mathbf{p}_{\Gamma_j - \sigma(s,j)}$.

Remark 2. $\sigma(s, j) \geq 0$ is a delay function, modeling the delay of the subdomain s at iteration j of the global problem.

The asynchronous iteration can be modeled as:

$$\left\{ \begin{array}{l} \mathbf{u}_{\Gamma_j}^G = \mathbf{S}^{G^{-1}}(\mathbf{b}^G + \mathbf{p}_{\Gamma_j}) \\ \text{If } s = 0 : \mathbf{q}_j^0 = \mathbf{S}^0(\mathbf{A}^{0T} \mathbf{u}_{\Gamma_j}^G - \mathbf{b}^{0,G}) \\ \text{If } s > 0 : \mathbf{q}_j^s = \begin{cases} \mathbf{J}^{sT} \mathbf{s}^{s,F} (\mathbf{J}^s \mathbf{A}^{sT} \mathbf{u}_{\Gamma_j - \sigma(s,j)}^G; \mathbf{f}^{s,F}) \text{ Updated} \\ \mathbf{q}_{j-1}^s, \text{ Not updated} \end{cases} \\ \mathbf{r}_j = - \left(\mathbf{A}^0 \mathbf{q}_j^0 + \sum_{s>0} \mathbf{A}^s \mathbf{q}_j^s \right) \\ \mathbf{p}_{\Gamma_{j+1}} = \mathbf{p}_{\Gamma_j} + \omega \mathbf{r}_j \end{array} \right. \tag{18}$$

For subdomains that were not updated: $\sigma(s, j) = \sigma(s, j - 1) + 1$.

It is crucial to note that if it exists, Subdomain 0 always contributes to the evaluation of the residual since computing \mathbf{q}_{j+1}^0 is only a post-processing of the Global solution. In order to unify notations, $\sigma(0, j) = 0$ is introduced, $\forall j$. Thus, the residual at the global iteration j is written in the asynchronous form:

$$\mathbf{r}_j = \sum_{s=0}^N \mathbf{A}^s \mathbf{J}^{sT} \mathbf{s}^{s,F} (\mathbf{J}^s \mathbf{A}^{sT} \mathbf{S}^{G^{-1}}(\mathbf{p}_{\Gamma_j - \sigma(s,j)} + \mathbf{b}^G); \mathbf{f}^{s,F}) \tag{19}$$

and then the asynchronous version of (12) can be given:

$$\mathbf{p}_{\Gamma_{j+1}} = \mathbf{p}_{\Gamma_j} - \omega \sum_{s=0}^N \mathbf{A}^s \mathbf{J}^{sT} \mathbf{s}^{s,F} (\mathbf{J}^s \mathbf{A}^{sT} \mathbf{S}^{G^{-1}}(\mathbf{p}_{\Gamma_j - \sigma(s,j)} + \mathbf{b}^G); \mathbf{f}^{s,F}) \tag{20}$$

Note that this expression is valid only after all local patches have at least contributed once to the estimation of the residual.

In order to ensure that at some point all patches provide new information, we assume that the **delay is bounded**:

$$\exists D \geq 0 \text{ such that } \forall (s, j), \sigma(s, j) \leq D \tag{21}$$

Proposition 1. The solution of the coupling problem (13) is a fixed point for any iteration in (20).

Proof. Let $\hat{\mathbf{p}}_{\Gamma}$ be the solution to the coupling problem as defined in (13):

$$\sum_{s=0}^N \mathbf{A}^s \mathbf{J}^{sT} \mathbf{s}^{s,F} (\mathbf{J}^s \mathbf{A}^{sT} \mathbf{S}^{G^{-1}}(\hat{\mathbf{p}}_{\Gamma} + \mathbf{b}^G); \mathbf{f}^{s,F}) = 0. \tag{22}$$

Then, if at some point $\forall k \in \{0, 1, \dots, D\}$, $\mathbf{p}_{\Gamma_{j-k}} = \hat{\mathbf{p}}_{\Gamma}$, the next iteration of (20) is $\mathbf{p}_{\Gamma_{j+1}} = \hat{\mathbf{p}}_{\Gamma}$ whatever the distribution of delays $(\sigma(s, j))$ among the subdomains, and by recursion, $\mathbf{p}_{\Gamma_{j+l}} = \hat{\mathbf{p}}_{\Gamma}$ for any $l > 0$. \square

For a given delay $0 \leq k \leq D$, we define $\varpi(k, j)$ as the set of subdomains (s) such that $\sigma(s, j) = k$. We define the contributions to the residual:

$$\begin{aligned} \mathbf{r}^s(\mathbf{p}_{\Gamma_{j-k}}) &= \mathbf{A}^s \mathbf{J}^{sT} \mathbf{s}^{s,F} (\mathbf{J}^s \mathbf{A}^{sT} \mathbf{S}^{G^{-1}}(\mathbf{p}_{\Gamma_{j-k}} + \mathbf{b}^G); \mathbf{f}^{s,F}) \\ &\quad - \mathbf{A}^s \mathbf{J}^{sT} \mathbf{s}^{s,F} (\mathbf{J}^s \mathbf{A}^{sT} \mathbf{S}^{G^{-1}}(\hat{\mathbf{p}}_{\Gamma} + \mathbf{b}^G); \mathbf{f}^{s,F}), \end{aligned} \tag{23}$$

and we use the short notation $\mathbf{r}_{j-k}^s = \mathbf{r}^s(\mathbf{p}_{\Gamma j-k})$. We have:

$$\mathbf{r}_j = \sum_{k=0}^D \sum_{s \in \varpi(k,j)} \mathbf{r}_{j-k}^s. \tag{24}$$

Writing $\mathbf{e}_j = (\mathbf{p}_{\Gamma j} - \hat{\mathbf{p}}_{\Gamma})$ the error at iteration j , we have:

$$\mathbf{e}_{j+1} = \mathbf{e}_j - \omega \sum_{k=0}^D \sum_{s \in \varpi(k,j)} \mathbf{r}_{j-k}^s. \tag{25}$$

In the linear case studied in [12], it was possible to give a simple link between \mathbf{r}_{j-k}^s and \mathbf{e}_{j-k} , which permitted to bring the convergence proof down to the spectral analysis of a certain linear operator. Such an approach is not possible here and we need to find a bounding of a well-chosen norm of the error.

Proposition 2 (General Error Bound). *The assumptions on the local models lead to $\mathbf{p}_{\Gamma} \mapsto \mathbf{r}^s(\mathbf{p}_{\Gamma})$ being strongly monotone and continuous, with associated constants given in (14) and (15), and we have:*

$$\begin{aligned} \|\mathbf{e}_{j+1}\|_G^2 &\leq \|\mathbf{e}_j\|_G^2 - 2\omega \underbrace{\left(\sum_{k=0}^D \sum_{s \in \varpi(k,j)} \gamma^s |\mathbf{A}^{sT} \mathbf{S}^{G^{-1}} \mathbf{e}_{j-k}|_{\mathbf{S}^s, G}^2 \right)}_a \\ &+ \omega^2 \underbrace{\left(N \sum_{k=0}^D \sum_{s \in \varpi(k,j)} M^s \|\mathbf{e}_{j-k}\|_G^2 + 2 \sum_{\substack{1 \leq k \leq D \\ 0 \leq q \leq D \\ 1 \leq K \leq k}} \sum_{\substack{s \in \varpi(k,j) \\ t \in \varpi(q, j-K)}} \sqrt{M^s M^t} \|\mathbf{e}_{j-K-q}\|_G \|\mathbf{e}_{j-k}\|_G \right)}_b. \end{aligned} \tag{26}$$

The proof is detailed in Appendix B.

This bound has two defects. First it mixes error terms from the previous 2D iterations. Second, the error is not correctly isolated in the first degree coefficient a of the bound (26) seem as a polynomial of degree two in ω . In order to prove the convergence, we need to find settings where a bound of the following form holds:

$$e_{j+1}^2 \leq e_j^2 (1 - 2\omega A + \omega^2 B) \quad \text{with } A > 0, \tag{27}$$

where e_j is some measure of the error at iteration j . Indeed, in that case, choosing $0 < \omega < 2A/B$ we have $(1 - 2\omega A + \omega^2 B) < 1$ and the iteration is a contraction. The process converges to the common fixed point. Note that the best convergence ratio is obtained for $\omega = A/B$, and it is worth $(1 - A^2/B)$.

In the next two subsections we analyze two configurations where the convergence can be proved.

3.3. Max norm on the history vector of the error

Following [42], the history vector of the error is introduced:

$$\hat{\mathbf{e}}_j^T = \left(\mathbf{e}_j^T \quad \mathbf{e}_{j-1}^T \quad \dots \quad \mathbf{e}_{j-2D}^T \right),$$

equipped with the max norm

$$\|\hat{\mathbf{e}}_j\|_{G, \infty} = \max_{0 \leq k \leq 2D} \|\mathbf{e}_{j-k}\|_G \tag{28}$$

Let \hat{k}_j be the delay for which the maximum is reached at iteration j .

This norm makes it trivial to bound the second degree term b (B.5) from above using (B.6):

$$b \leq \underbrace{\left(N \sum_{k=0}^D \sum_{s \in \varpi(k,j)} M^s + 2 \sum_{\substack{1 \leq k \leq D \\ 0 \leq q \leq D \\ 1 \leq K \leq k}} \sum_{\substack{s \in \varpi(k,j) \\ t \in \varpi(q, j-K)}} \sqrt{M^s M^t} \right)}_{B_j} \|\hat{\mathbf{e}}_j\|_{G, \infty}^2. \tag{29}$$

To bound a from below:

$$a \geq \sum_{k=0}^D \sum_{s \in \varpi(k,j)} \gamma^s |\mathbf{A}^{sT} \mathbf{S}^{G^{-1}} \mathbf{e}_{j-k}|_{\mathbf{S}^s, G}^2 \geq \sum_{s \in \varpi(\hat{k}_j, j)} \gamma^s |\mathbf{A}^{sT} \mathbf{S}^{G^{-1}} \mathbf{e}_{j-\hat{k}_j}|_{\mathbf{S}^s, G}^2. \tag{30}$$

We need to further strengthen hypothesis (21) by assuming that sufficiently many subdomains are activated for the \hat{k}_j contribution so that the following bounding exists:

$$\sum_{s \in \varpi(\hat{k}_j, j)} \gamma^s \left| \mathbf{A}^{sT} \mathbf{S}^{G^{-1}} \mathbf{e}_{j-\hat{k}_j} \right|_{\mathbf{S}^s, G}^2 \geq \underbrace{\frac{\theta_{\hat{k}_j, j}}{\kappa}}_{A_j} \left\| \mathbf{e}_{j-\hat{k}_j} \right\|_G^2, \quad (31)$$

where $\theta_{\hat{k}_j, j}$ is the minimal non-zero eigenvalue of the matrix:

$$\mathbf{S}^{G^{-1}} \left(\sum_{s \in \varpi(\hat{k}_j, j)} \gamma^s \mathbf{A}^s \mathbf{S}^s, G \mathbf{A}^{sT} \right),$$

and where $\kappa \geq 1$ is some constant, which can be illustrated by the following cases:

- $\kappa = 1$ would be suited to $\mathbf{e}_{j-\hat{k}_j}$ being non-zero only on the boundary of $\bigcup_{s \in \varpi(\hat{k}_j, j)} \Omega^s$.
- $\kappa = N$ would correspond to one subdomain being activated with the \hat{k}_j and the error $\mathbf{e}_{j-\hat{k}_j}$ being smoothly distributed on the domain.

In practice, κ can be influenced by the load balancing between patches, and hardware properties like the speed of the network.

Theorem 1. *Under the monotonicity and continuity hypotheses of Section 2.5.5 together with the bounded delay assumption (21) and its reinforcement (31), there exists a non-empty interval of the form $(0, \omega_1)$ for the relaxation coefficient for which the asynchronous iteration converges.*

Proof. Introducing $A = \min A_j > 0$ and $B = \max B_j$ taken among all the potential distribution of delays in the subdomains, we have:

$$\left\| \mathbf{e}_{j+1} \right\|_G^2 \leq \left\| \hat{\mathbf{e}}_j \right\|_{G, \infty}^2 (1 - 2\omega A + B\omega^2), \quad (32)$$

for $0 < \omega < \omega_1 = 2A/B$, we have:

$$\begin{aligned} \left\| \mathbf{e}_{j+1} \right\|_G^2 &< \left\| \hat{\mathbf{e}}_j \right\|_{G, \infty}^2 \\ \implies \left\| \hat{\mathbf{e}}_{j+2D} \right\|_{G, \infty}^2 &< \left\| \hat{\mathbf{e}}_j \right\|_{G, \infty}^2. \end{aligned} \quad (33)$$

Thus the error (strictly) decreases at least every $2D$ iteration. \square

However, the convergence in max-norm over an interval of $2D$ global iterations opens the possibility for saw-tooth convergence with decreasing peaks.

3.4. Sufficient condition for monotone convergence

It is possible to recover a strict decrease of the error at each iteration (and not over a $2D$ interval) assuming that enough fresh information is provided. That is to say when equation (31) applies to the previous iteration. This occurs in particular in the case where patches $(\Omega^s)_{s>0}$ are non-adjacent and therefore are all connected to the subdomain Ω^0 . Beside being in contact with the whole interface (the interface degrees of freedom can be ordered such that $\mathbf{A}^0 = \mathbf{I}$ and $\mathbf{J}^0 = \mathbf{I}$), subdomain Ω^0 is always synchronous with the global problem. Thus, when Subdomain Ω^0 exists, the bounding from below is simple to obtain:

$$\begin{aligned} \sum_{k=0}^D \sum_{s \in \varpi(k, j)} \langle \mathbf{e}_{j-k}, \mathbf{r}_{j-k}^s \rangle_G &\geq \sum_{s \in \varpi(0, j)} \langle \mathbf{e}_j, \mathbf{r}_j^s \rangle_G \\ &\geq \gamma^0 \left\| \mathbf{S}^{G^{-1}} \mathbf{e}_j \right\|_{\mathbf{S}^0, G}^2 \geq \underbrace{\theta^0}_A \left\| \mathbf{e}_j \right\|_G^2 \end{aligned} \quad (34)$$

where $\theta^0 > 0$ is the minimal eigenvalue of the matrix $\gamma^0 \mathbf{S}^0 \mathbf{S}^{G^{-1}} \mathbf{S}^{0, G}$.

Remark 3. Note that the same property can be obtained with contiguous patches by forcing the global model to wait for enough new data be provided by patches.

The bounding from above of the b term is a bit more complex, because of the many delayed error terms. Let us prove that there exists some interval $(\omega_{\min}, \omega_{\max})$ for which the relaxed iteration is strictly decreasing, in the sense that there exists $1 > c > 0$, which depends on ω , such that, $\forall j$:

$$\left\| \mathbf{e}_{j+1} \right\|_G^2 \leq c \left\| \mathbf{e}_j \right\|_G^2 \quad (35)$$

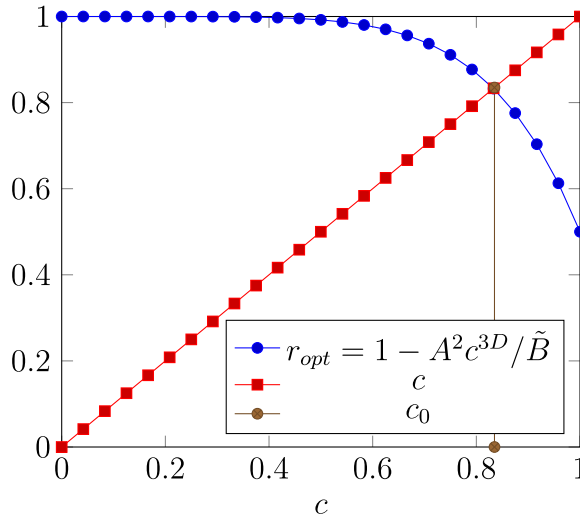


Fig. 2. Typical dependence of rate of convergence vs c

Let us assume that such a constant c exists. We have:

$$\begin{aligned}
 b &\leq N \sum_{k=0}^D \sum_{s \in \sigma(k,j)} M^s \|\mathbf{e}_{j-k}\|_G^2 + 2 \sum_{\substack{1 \leq k \leq D \\ 0 \leq q \leq D \\ 1 \leq K \leq k}} \sum_{\substack{s \in \sigma(k,j) \\ t \in \sigma(q,j-K)}} \sqrt{M^s M^t} \|\mathbf{e}_{j-K-q}\|_G \|\mathbf{e}_{j-k}\|_G \\
 &\leq \left(N \sum_{k=0}^D \sum_{s \in \sigma(k,j)} M^s c^{-2k} + 2 \sum_{\substack{1 \leq k \leq D \\ 0 \leq q \leq D \\ 1 \leq K \leq k}} \sum_{\substack{s \in \sigma(k,j) \\ t \in \sigma(q,j-K)}} \sqrt{M^s M^t} c^{-(k+K+q)} \right) \|\mathbf{e}_j\|_G^2 \\
 &\leq \underbrace{\left(N \sum_{k=0}^D \sum_{s \in \sigma(k,j)} M^s + 2 \sum_{\substack{1 \leq k \leq D \\ 0 \leq q \leq D \\ 1 \leq K \leq k}} \sum_{\substack{s \in \sigma(k,j) \\ t \in \sigma(q,j-K)}} \sqrt{M^s M^t} \right)}_{\tilde{B}_j} c^{-3D} \|\mathbf{e}_j\|_G^2
 \end{aligned} \tag{36}$$

Introducing $\tilde{B} = \max \tilde{B}_j$, taken among all the potential distributions of delays in the subdomains:

$$\|\mathbf{e}_{j+1}\|_G^2 \leq \|\mathbf{e}_j\|_G^2 (1 - 2\omega A + \omega^2 \tilde{B} c^{-3D}) \tag{37}$$

Theorem 2. Under the monotonicity and continuity hypotheses of Section 2.5.5 together with the bounded delay assumption (21) and the assumption of non-connected patches leading to the bound (34), there exists a non-empty interval of the form $(\omega_{\min}, \omega_{\max})$ for the relaxation coefficient for which the asynchronous iteration converges with monotone decrease of the error.

Proof. For a given problem, it is possible to evaluate A , \tilde{B} and D . For (37) to be consistent with (35), we need to find a non-empty domain for ω and $0 < c < 1$ such that:

$$1 - 2\omega A + \omega^2 \tilde{B} c^{-3D} < c \tag{38}$$

For a given c , the optimal rate of convergence is attained for $\omega_{opt} = Ac^{3D}/\tilde{B}$, and it is worth $r_{opt}(c) = (1 - \frac{A^2 c^{3D}}{\tilde{B}})$. Fig. 2 illustrates the existence of a domain $(c_0, 1)$ where $c \in (c_0, 1) \Rightarrow c \geq r_{opt}(c)$. $c_0 > 0$ is the solution to $1 - A^2 c_0^{3D}/\tilde{B} = c_0$.

For a given $c \in (c_0, 1)$, let $\delta = A^2 - (1 - c)\tilde{B}c^{-3D} > 0$, any $\omega \in (\frac{A-\sqrt{\delta}}{\tilde{B}c^{-3D}}, \frac{A+\sqrt{\delta}}{\tilde{B}c^{-3D}})$ satisfies (38) and leads to a convergence rate in $(r_{opt}(c), c)$ at each iteration.

We set $\omega_{\min} = Ac_0^{3D}/\tilde{B}$ and $\omega_{\max} = A/\tilde{B}$. For $\omega \in (\omega_{\min}, \omega_{\max})$, the rate of convergence between two consecutive iterations is by construction at least $(\omega\tilde{B}/A)^{1/(3D)} < 1$. \square

Contrarily to the synchronous case, or to the linear analysis of [12], the difficulty is that the relaxation cannot be too small (else saw-tooth convergence of Theorem 1 would be recovered). Also, for large D the result may become unpractical as the interval of monotone convergence would be quite small and the convergence rate very close to 1. Note that anyhow, the analysis is based on

a worst case scenario and the width of the actual interval of monotone convergence can be much larger and the convergence rate much better than the bound.

3.5. Practical considerations about elastoplasticity

Plasticity needs to introduce internal variables (like plastic strain or hardening), the evolution of which depends on the load history. For instance, the assessment of fatigue requires simulating lots of cyclic loads themselves decomposed into many increments. The classical solution strategy is a step-by-step procedure (time outer iteration) where each time step is a nonlinear problem solved by a Newton–Raphson algorithm (inner iteration) that alternates between return mapping (to update the hardening at the Gauss points) and tangent solves (to update the displacement).

The first approach to combine plasticity with global–local coupling is to use it at each load increment. In [2], such an incremental global–local procedure is interpreted as a modified Newton approach. One computational interest of this technique is to confine the nonlinear solves into the patches.

A second possibility is to treat the whole time interval inside the domains, in a manner similar to the Schwarz waveform relaxation techniques [46]. At each global–local iteration, the global domain solves a family of linear systems corresponding to all the time steps with adapted external and interface load. Since it is linear, a multiple right-hand side strategy is possible. The global model then transmits a time sequence of Dirichlet conditions to be imposed on the patches. The patches independently solve the Dirichlet problem while updating their internal variables in accordance with the nonlinear evolution. This approach leads to a much higher degree of parallelism with more independent computations. It was used in a simplified way in [7] for elastoviscoplastic problems where the models were allowed to adapt their increments (cutbacks) independently of the global model. Note that this approach is covered by the theory above by concatenating all the time steps (t_0, \dots, t_n) together and using a time-integrated norm:

$$\underline{\mathbf{p}}_r = \begin{pmatrix} \mathbf{p}_r^{t_0} \\ \vdots \\ \mathbf{p}_r^{t_n} \end{pmatrix}, \quad \|\underline{\mathbf{p}}_r\|^2 = \sum_{j=0}^n \|\mathbf{p}_r^{t_j}\|_G^2. \quad (39)$$

4. Assessments

We illustrate the convergence of the asynchronous global–local coupling on two academic examples. Note that by essence, the numerical experiments are not strictly reproducible since the resolution process depends on the availability of the data, which cannot be controlled. Asynchronous computations are thus always executed three times and the mean values are retained (standard deviation is negligible).

In our comparison, we retained the Aitken accelerated synchronous iteration as our reference solver because of its excellent efficiency. Aitken’s Δ^2 can be viewed as a technique to dynamically adapt (*i.e.* at each iteration) the relaxation coefficient. For now, we do not have equivalent techniques for asynchronous iterations, and we identified the “optimal” relaxation coefficient by trial and error.

4.1. Cluster

The studies were carried out with the cluster of the LMPS simulation center using several workstations connected by an Ethernet network. These machines are quite heterogeneous with 4 different generation of CPUs:

- Intel(R) Xeon(R) CPU E5-1660 v3 (Haswell) @ 3.00 GHz (8 cores)
- Intel(R) Xeon(R) CPU E5-2630 v4 (Broadwell) @ 2.20 GHz (10 cores)
- Intel(R) Xeon(R) Silver 4116 CPU (Skylake) @ 2.10 GHz (12 cores)
- Intel(R) Xeon(R) W-2255 CPU (Cascade Lake) @ 3.70 GHz (10 cores)

Besides the heterogeneity, another characteristic is that the cluster can be used by several users simultaneously, there is no queuing system.

We use one MPI process for the global problem and as many processes as needed to distribute the local problems according to the study. As much as possible the MPI processes are allocated to the cores of the same CPUs.

The presence of the Ethernet network prevents the full use of the RDMA features. In order to avoid hidden synchronization due to the implementation of the MPI methods, we had to slightly modify our algorithm: instead of testing for the availability of new data, the solvers never stop computing with the available information even if nothing new was put, which may lead to solving twice the same system. This phenomena will be observable in the performance tables where we give the number of global iterations as well as the minimal and maximal number of solves in the fine patches.

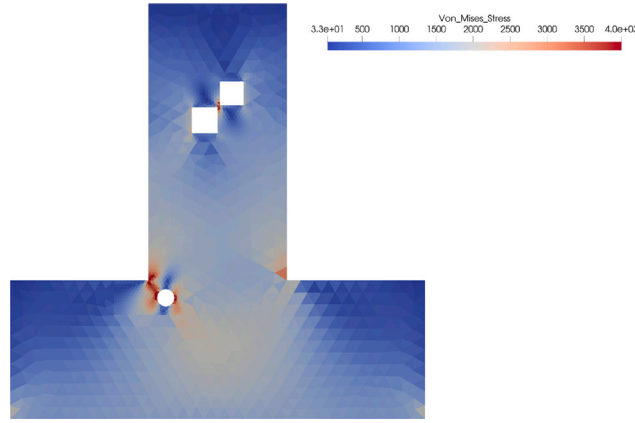


Fig. 3. Von Mises stress at the convergence.

4.2. Plasticity system

For our illustrations, we focus on associated elastoplasticity problems. In this context, the global problem is assumed to be a linear elasticity problem, while the local problems exhibit nonlinear elastoplastic behavior with linear kinematic and isotropic hardening. The governing equations for the local problem can be stated as follows:

$$\begin{aligned}
 &\text{Find } u : \Omega \subset \mathbb{R}^d \rightarrow \mathbb{R}^d, \\
 &\text{div}(\sigma) + f = 0 \quad \text{in } \Omega, \\
 &u = 0 \quad \text{on } \partial_d \Omega, \\
 &\sigma \cdot n = 0 \quad \text{on } \partial \Omega \setminus \partial_d \Omega, \\
 &\varepsilon(u) = \nabla^{sym} u = \varepsilon^e + \varepsilon^p, \\
 &\sigma = \frac{E}{1+\nu} \left(\varepsilon^e + \frac{\nu}{1-2\nu} \text{tr}(\varepsilon^e) I \right), \\
 &\text{Yield function } Y(\sigma, \alpha) = \|\text{Dev}(\sigma - \frac{2}{3} H_k \varepsilon^p)\| - \sqrt{\frac{2}{3}} (\sigma_{y0} + H_i \alpha) \leq 0.
 \end{aligned} \tag{40}$$

Here, u represents the displacement vector field, σ is the Cauchy stress tensor, and $f \neq 0$ represents the body force. Dirichlet boundary condition $u = 0$ is imposed on $\partial_d \Omega$, and Neumann boundary condition $\sigma \cdot n = 0$ on $\partial \Omega \setminus \partial_d \Omega$. The strain tensor $\varepsilon(u)$ (symmetric part of the gradient of displacement) is decomposed into the elastic part ε^e and the plastic part ε^p . The stress–strain relation is given by the constitutive law, and the yield function $Y(\sigma, \alpha)$ characterizes the plastic behavior (Dev operator extracts the deviatoric part of a tensor). The model considers linear kinematic and isotropic hardening, where H_i and H_k are the associated hardening modulus, σ_{y0} is the uniaxial yield stress. The solution technique for this problem uses a θ -scheme for the pseudo-time integration, and it is readily available in the GetFEM software. We use the default solver configuration ($\theta = 1$ aka backward Euler method).

In the following analysis, we consider only one load increment, and the body load is adjusted to trigger plasticity in the patches. In future work, the asynchronous approach can be extended to parallelization in time using Schwarz waveform relaxation.

4.3. Two-dimensional illustration

The first test case, Fig. 1, is inspired from [2]. The structure is composed of five unit-length squares arranged in a T-shape. The global mesh contains 700 nodes and a complement zone (subdomain Ω^0) represented in yellow in the global model. There are two zones of interest in which complex geometrical details are added. In the green zone of interest, the addition of 1 circular hole and a modification at the boundary of the global structure can be seen. The addition of two square voids characterizes the red patch inside the structure. The Fine models have refined meshes (380 nodes each). We use the plane strain assumption. The elastic behavior is given by the following Lamé coefficients: shear modulus $\mu = 80769$ and first coefficient $\lambda = 121150$. Regarding plasticity, we use $\sigma_{y0} = 4000$ which results in an elastic limit of 3266. The kinematic and isotropic hardening coefficients are $H_k = 16$ and $H_i = 20$. The solid is clamped on its bottom face, while the body load is worth 0 in the x direction and 1300 in the y direction.

Fig. 3 illustrates the von Mises stress obtained through the global–local iteration process. The maximum value of the von Mises stress in one of the patches is 4000 and 3800 respectively, far exceeding the elastic limit. 4 shows the hardening in both local problems where we can see that we achieve the plastic regime.

This simple example is not advantageous for the asynchronous iteration because all systems are solved quasi-instantaneously. We mostly use it to illustrate the difference of convergence behavior as explained in Sections 3.3 and 3.4. Indeed, the presence of the complement domain Ω^0 makes it possible to find a relaxation coefficient which leads to monotone convergence.

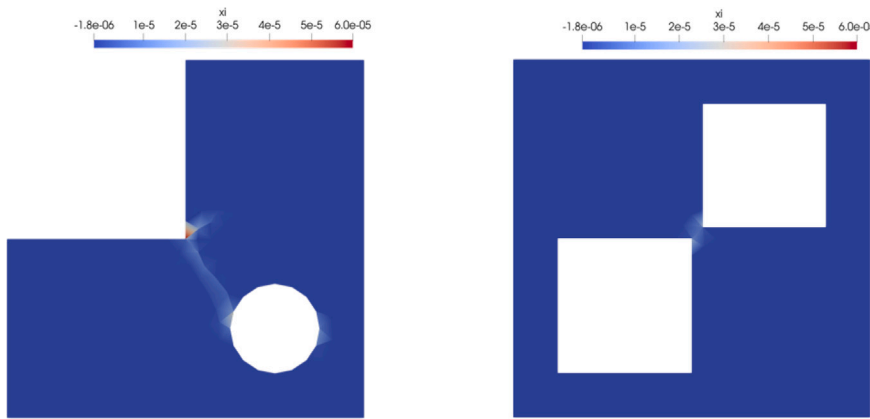


Fig. 4. Accumulated plasticity in the local problems.

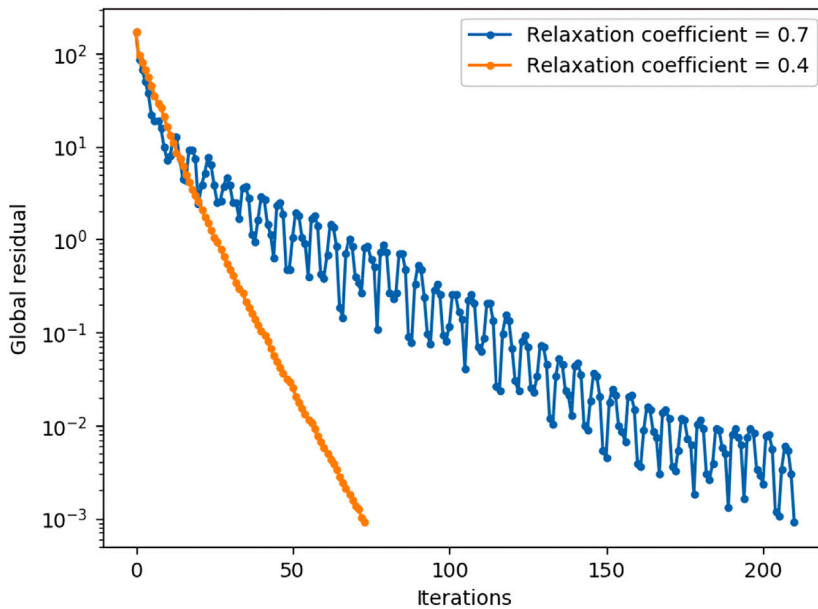


Fig. 5. The impact of the relaxation coefficient on the convergence.

In Fig. 5, we compare the convergence (decrease of the norm of the residual) along iterations for two values of the relaxation parameter $\omega = 0.7$ and $\omega = 0.4$. In the first case, we observe the saw-tooth convergence: the maximum delay is around $D = 4$, the residual decreases with micro-variations of a factor of 10, while the general trend (shown by the upper peaks) is towards zero. In the second case, the relaxation is adapted for the iteration to enter the domain of monotone convergence, and in this case more efficient, regime.

4.4. Three-dimensional test case

The global–local coupling method is primarily a non-invasive multi-level modeling technique. As such, its computational performance is difficult to quantify. As we have no industrial test case to handle, we generate an easy to customize three-dimensional test case with the objective to generate as many patches as wished. Since it seems unnatural to accumulate more patches than necessary on a given geometry, we particularly focus on the ability to handle structures of increasing size (and more patches). Even if this kind of study is related to weak scalability, the global–local coupling is not a competitor to high performance domain decomposition methods.

The domain is chosen to be a right-angled parallelepiped covered by non-overlapping contiguous unit-length cuboid patches. Figs. 6(a) and 6(b) show the 8- and 16-subdomain cases. In that case there is no complement zone $\Omega^0 = \emptyset$. The left side of the domain is clamped and a constant body load is applied, adjusted to trigger plasticity.

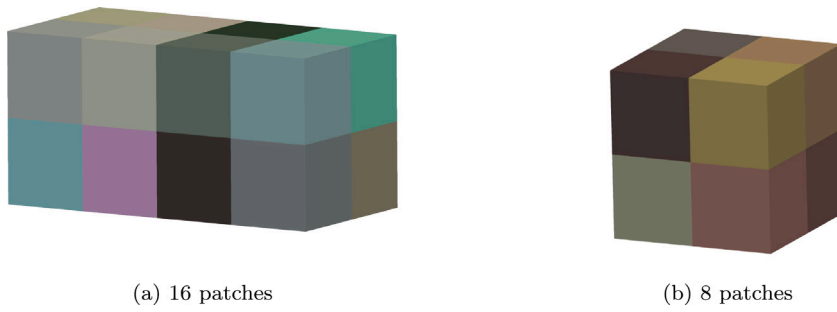


Fig. 6. fig:3D academic case.

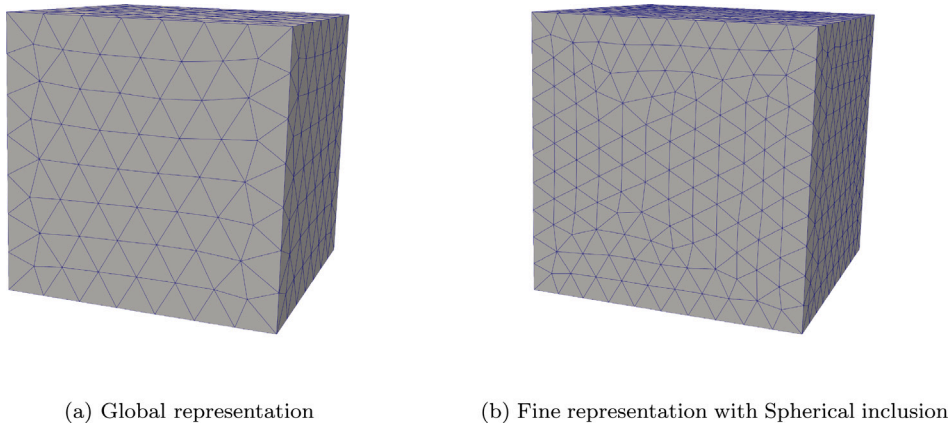


Fig. 7. Example of one unit cube with different representations.

Table 1

Mesh data for 128 subdomains.

Problem	Global	Local (One subdomain)
Number of nodes	2769	1254

The global version of the cuboids is a homogeneous isotropic linear elastic solid (Young modulus $E = 10000$, Poisson’s coefficient $\nu = 0.3$) with a coarse mesh, see Fig. 7(a). The local model in the cuboids is heterogeneous with a linear elastic matrix (same material as the Global model) and a central elastoplastic inner sphere (with diameter half the side of the cube, same elastic constant as the matrix, and same plastic properties as previous example $\sigma_{y0} = 4000$, $H_k = 16$ and $H_l = 20$), see Figs. 7(b). A refined mesh is used in the local patches, adjacent fine meshes are not necessarily matching at the interface. In contrast, the global mesh is conforming at the interface.

The body load is of the form $g * (1, 1, 1)$, it is adjusted depending on the test case in order to ensure that all sphere undergo plastic evolution. Depending on the number of subdomains, it ranges from $g = 1900$ to $g = 10000$. This setting leads to subdomains closer to the clamped boundary undergoing higher level of plasticity than others.

4.4.1. Preliminary study

The preliminary study was conducted on a 128-patch ($4 \times 4 \times 8$) geometry, with the mesh dimensions provided in Table 1. The focus of the study was on cases where the load imbalance arises from the intensity of nonlinearity.

Table 2 displays the performance results. The asynchronous approach with optimal relaxation parameter ω_{opt} exhibited improved performance compared to the synchronous Aitken acceleration. The time was reduced by a factor of three, whereas the number of global iterations was more than tripled proving the noxiousness of synchronization in codes. As can be observed, local patches had enough time to carry many resolutions, in particular the ones which remained in the elastic domain (roughly 4 times more computations).

The same study was repeated on a 256-patch ($4 \times 4 \times 16$) geometry, with mesh data provided in Table 3. Table 4 presents the results. Here again, the asynchronous approach also demonstrated improved performance compared to the synchronous Aitken acceleration.

The consistent trend across both cases was that the asynchronous approach with the optimal relaxation parameter ω_{opt} achieved reduced computation times compared to the synchronous Aitken acceleration. This observation emphasizes the advantage of allowing

Table 2
Iterations & Time (Nonlinear plastic inclusion).

Variant	Sync. Aitken	Async. ω_{opt}
Time(s)	508	155
#iter. glob.	25	84
#loc. sol. [min, max]	.	[119 - 428]

Table 3
Mesh data for 256 subdomains.

Problem	Global	Local (One subdomain)
Number of nodes	5490	2308

Table 4
Iterations & Time (Nonlinear plastic inclusion).

Variant	Sync. Aitken	Async. ω_{opt}
Time(s)	703	403
#iter. glob.	30	95
#loc. sol. [min, max]	.	[181 - 594]

Table 5
Number of nodes in the meshes for the weak scalability study.

# of subdomains	8	27	64	125	216	343
Global	233	667	1449	2681	4465	6903
Local (1 subdomain)	1858	1858	1858	1858	1858	1858

Table 6
Weak scalability: Number of iterations in the elastoplastic case.

#patches	8	27	64	125	216	343
Aitken #iter.	25	23	23	25	26	27
Async. #glob. sol.	1083	72	77	81	99	96
Async. #loc. sol. [min, max]	[68, 191]	[84, 183]	[106, 241]	[126, 490]	[152, 410]	[178, 518]

subdomains to work independently, free from strict synchronization. While initially counterintuitive, the increased number of global iterations was effectively compensated by the overall reduction in computation time.

Furthermore, the wide range of local subdomain computational load in the asynchronous approach, as indicated by the [min, max] values, underscores the method’s adaptability. Different subdomains may converge at varying rates due to nonlinearity. However, the asynchronous approach effectively manages these variations, with subdomains in the elastic domain converging faster and those with stronger nonlinearity requiring more iterations.

In conclusion, the preliminary study confirms the merits of the asynchronous global–local non-invasive coupling method with the optimal relaxation parameter in addressing nonlinear plasticity problems with multiple patches. The asynchronous approach offers improved computation time, making it a promising solution for efficiently tackling large-scale and complex problems.

4.4.2. Weak scalability

In this subsection, a study of weak scalability is conducted to assess the performance of the method. A cubic geometry, as shown in Fig. 6(b), is maintained while multiplying patches. The cases consist of n^3 ($n \in \{2, 3, \dots, 7\}$) patches. The domain size increases with the number of subdomains, following the standard practice for weak scalability assessment of domain decomposition methods. Again, the global model is linear, while the local models feature elastoplastic spherical inclusions.

The patches are not identical in terms of meshes, but they are well-balanced in terms of degrees of freedom. As the study progresses, the global model increases in size, starting from being 8 times smaller than one patch and ending up 3.7 times larger. Table 5 summarizes the number of nodes for each case.

To provide an illustration, Figs. 9(a) and 9(b) display the von Mises stress and the hardening in the case with eight subdomains. It demonstrates that all spherical inclusions reach their elastic limit, with a large values difference.

Examining Fig. 8, we notice a general trend as the number of patches increases. The computation time for the asynchronous method increases more slowly than for the synchronous method (Aitken). This indicates that the asynchronous method exhibits better scalability in terms of computation time as the problem becomes larger.

Looking at Table 6, we observe that the number of global iterations for the asynchronous method (Async. #iter. glob.) decreases significantly as the number of patches increases. This means that for larger problems, the asynchronous method requires fewer global iterations to achieve convergence.

On the other hand, the number of iterations for the synchronous method (Aitken #iter.) remains relatively constant or slightly increases with the number of patches. This suggests that the synchronous method requires more global iterations for larger problems, which can lead to a significant increase in computation time.

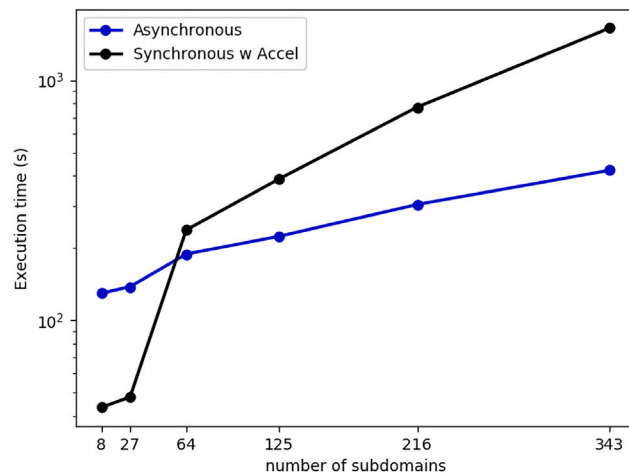


Fig. 8. Weak scalability: time in the plasticity case.

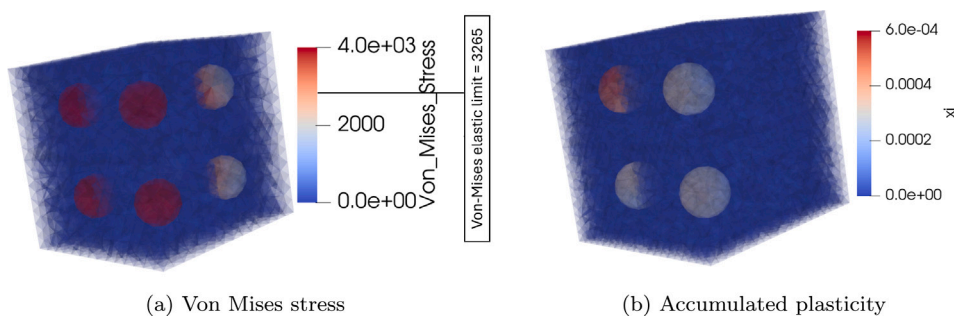


Fig. 9. Mechanical fields in the 8-subdomain case.

Table 6 also shows a range of values for local computation time (Async. #loc. sol. [min, max]). This variability is observed in the asynchronous method because subdomains perform their local computations at different rates. Some subdomains may require more iterations to converge due to the influence of nonlinearities and plasticity, resulting in longer solution times. On the other hand, subdomains that remain in the elastic domain converge faster and require fewer iterations.

5. Conclusion

This article focused on the application of an asynchronous global–local non-invasive coupling method to nonlinear monotone patches, in the interest to introduce elastoplastic patches in a linear elastic global model. The study presented an asynchronous version of the non-intrusive global–local coupling method. The convergence of the discrete system was proved using paracontractions techniques.

Furthermore, the implementation of the method with MPI RDMA parallelization was discussed, enabling efficient distributed computation. Assessments were conducted on problems involving a significant number of patches, demonstrating the effectiveness of the coupling approach. Notably, the asynchronous method, employing hand-tuned relaxation, exhibited superior performance in terms of computation time compared to the synchronous solver with Aitken’s dynamic relaxation on a cluster of heterogeneous machines.

In future studies, we will focus on the development of efficient estimation techniques for the optimal relaxation parameter in the asynchronous iteration. This would enhance the overall performance and effectiveness of the method.

CRedit authorship contribution statement

Ahmed El Kerim: Writing – original draft, Software, Methodology, Conceptualization. **Pierre Gosselet:** Writing – review & editing, Software, Resources, Methodology, Conceptualization. **Frédéric Magoulès:** Writing – review & editing, Resources, Methodology, Conceptualization.

Declaration of competing interest

The authors declare that they have no known competing financial interests or personal relationships that could have appeared to influence the work reported in this paper.

Data availability

Data will be made available on request.

Acknowledgments

This work was partly funded by the French National Research Agency as part of project ADOM, under grant number ANR-18-CE46-0008.

Appendix A. Properties of the condensed operators

A.1. Subdomain's equation

For some subdomain $\omega \subset \mathbb{R}^d$, we consider a variational formulation of the form $a(u, v) = l(v)$ in the Hilbert subspace $\mathcal{U} \subset H^1(\omega)^d$ which accounts for the zero Dirichlet conditions. l is assumed to be a continuous linear form in \mathcal{U} and to embed non-zero Dirichlet conditions thanks to an extension. The left-hand side a is linear in the second variable, it is of the form:

$$\begin{aligned} u &\in H^1(\Omega^s), \forall v \in H^1(\Omega^s) \\ a^F(u, v) &:= \int_{\omega} \sigma(\varepsilon(u)) : \varepsilon(v) dx \end{aligned} \quad (\text{A.1})$$

where the Cauchy stress tensor σ is a nonlinear function of the symmetric gradient $\varepsilon(u)$. For better readability, internal variables that account for the hardening are omitted.

The monotonicity means:

$$\exists \gamma > 0, \quad \forall (u, v) \in H^1(\omega), a(u, u - v) - a(v, u - v) \geq \gamma \|u - v\|_{\mathcal{U}}^2, \quad (\text{A.2})$$

where we used the H^1 seminorm $\|u\|_{\mathcal{U}}^2 = \int_{\omega} \|\varepsilon(u)\|^2 dx$. This property is encountered for elastoplastic models with positive hardening, see [38, lemma 2].

The Lipschitz continuity means:

$$\exists M > 0, \quad \forall (u_1, u_2, v) \in H^1(\omega), a(u_1, v) - a(u_2, v) \leq M \|u_1 - u_2\|_{\mathcal{U}} \|v\|_{\mathcal{U}}. \quad (\text{A.3})$$

Note that weaker continuity assumptions are possible, see [6] for instance.

In any case, we can use the following global model:

$$a^G(u, v) = \int_{\omega} (H : \varepsilon(u)) : \varepsilon(v) dx. \quad (\text{A.4})$$

H is the (symmetric definite positive) Hooke tensor. a^G is a bilinear continuous semi-coercive form which is equivalent to the H^1 seminorm.

A.2. Dirichlet problem on the fine subdomain

Let $\Gamma \subset \partial\omega$ be the interface of the subdomain and \mathcal{U}_{Γ} the trace space of \mathcal{U} . \mathcal{U}_{Γ} is a Hilbert space and $\|\text{tr}(u)\|_{\mathcal{U}_{\Gamma}} \leq \|u\|_{\mathcal{U}}$. Using a Lagrangian approach, the Dirichlet problem can be written as:

$$\begin{aligned} &\text{Given } u_{\Gamma} \in \mathcal{U}_{\Gamma}, \text{ find } u \in \mathcal{U}, \lambda \in \mathcal{U}_{\Gamma}^*, \text{ such that} \\ &\begin{cases} a(u, v) - \langle \lambda, \text{tr}(v) \rangle_{\Gamma} = l(v), & \forall v \in \mathcal{U} \\ \langle \mu, u_{\Gamma} - \text{tr}(u) \rangle_{\Gamma} = 0, & \forall \mu \in \mathcal{U}_{\Gamma}^* \end{cases} \end{aligned} \quad (\text{A.5})$$

For the given hypotheses, this is a well-posed problem and the Dirichlet-to-Neumann map s is well-defined:

$$\begin{aligned} s : \mathcal{U}_{\Gamma} &\rightarrow \mathcal{U}_{\Gamma}^* \\ u_{\Gamma} &\mapsto s(u_{\Gamma}) = \lambda \text{ solution to (A.5),} \end{aligned} \quad (\text{A.6})$$

more, it is continuous (in the dual norm) and monotone.

A.3. Dirichlet problem on the global model of the subdomain

This situation is more classical. We can invoke the Lax–Milgram theorem to prove the existence of the solution to the Dirichlet problem, the continuity of the solution w.r.t the Dirichlet condition, the existence of the Dirichlet-to-Neumann map and the fact that it inherits linearity, symmetry, (semi) coercivity and continuity from the form in the subdomains. This leads to the Dirichlet-to-Neumann map defining a norm on the trace space which is equivalent to the natural norm. This makes it legitimate to express the monotonicity and continuity properties of the fine condensed operators in terms of subdomains’ coarse (global) Dirichlet-to-Neumann map.

A.4. Discretization

We use the classical Galerkin finite element approach. Let \mathcal{U}_h be a finite-dimension subspace of \mathcal{U} and ϕ be the matrix of shape functions so that any field $u_h \in \mathcal{U}_h$ can be written in terms of its vector of degrees of freedom \mathbf{u} : $u_h = \phi\mathbf{u}$. We can define the vector of internal forces f_{int}^F and the stiffness matrix \mathbf{K}^G :

$$\forall(\mathbf{u}, \mathbf{v}), \quad \mathbf{v}^T \mathbf{f}_{int}^F(\mathbf{u}) = a^F(\phi\mathbf{u}, \phi\mathbf{v})$$

$$\mathbf{v}^T \mathbf{K}^G \mathbf{u} = a^G(\phi\mathbf{u}, \phi\mathbf{v}) \tag{A.7}$$

It can be checked that monotonicity and continuity are preserved during discretization. Also, the discrete Dirichlet-to-Neumann maps of Eqs. (10) and (11) are well-defined and possess the required properties.

Appendix B. Proof of Proposition 2

Due to Eq. (25):

$$\|\mathbf{e}_{j+1}\|_G^2 = \|\mathbf{e}_j\|_G^2 - 2\omega \sum_{k=0}^D \sum_{s \in \varpi(k,j)} \langle \mathbf{e}_j, \mathbf{r}_{j-k}^s \rangle_G + \omega^2 \left\| \sum_{k=0}^D \sum_{s \in \varpi(k,j)} \mathbf{r}_{j-k}^s \right\|_G^2. \tag{B.1}$$

The first degree term needs to be further analyzed in order to make appear terms with the same delay. The recursion is obtained with:

$$\mathbf{e}_j = \mathbf{e}_{j-1} - \omega \left(\sum_{q=0}^D \sum_{s \in \varpi(q,j-1)} \mathbf{r}_{j-1-q}^s \right)$$

$$= \mathbf{e}_{j-k} - \omega \left(\sum_{K=1}^k \sum_{q=0}^D \sum_{t \in \varpi(q,j-K)} \mathbf{r}_{j-K-q}^t \right). \tag{B.2}$$

Hence:

$$\sum_{k=0}^D \sum_{s \in \varpi(k,j)} \langle \mathbf{e}_j, \mathbf{r}_{j-k}^s \rangle_G = \sum_{k=0}^D \sum_{s \in \varpi(k,j)} \langle \mathbf{e}_{j-k}, \mathbf{r}_{j-k}^s \rangle_G$$

$$- \omega \sum_{k=1}^D \sum_{s \in \varpi(k,j)} \sum_{K=1}^k \sum_{q=0}^D \sum_{t \in \varpi(q,j-K)} \langle \mathbf{r}_{j-K-q}^t, \mathbf{r}_{j-k}^s \rangle_G. \tag{B.3}$$

Finally, Eq. (B.1) can be written as:

$$\|\mathbf{e}_{j+1}\|_G^2 = \|\mathbf{e}_j\|_G^2 - 2\omega \underbrace{\sum_{k=0}^D \sum_{s \in \varpi(k,j)} \langle \mathbf{e}_{j-k}, \mathbf{r}_{j-k}^s \rangle_G}_a$$

$$+ \omega^2 \left(\underbrace{\left\| \sum_{k=0}^D \sum_{s \in \varpi(k,j)} \mathbf{r}_{j-k}^s \right\|_G^2}_{b} + 2 \sum_{k=1}^D \sum_{s \in \varpi(k,j)} \sum_{K=1}^k \sum_{q=0}^D \sum_{t \in \varpi(q,j-K)} \langle \mathbf{r}_{j-K-q}^t, \mathbf{r}_{j-k}^s \rangle_G \right). \tag{B.4}$$

Using convexity and Cauchy–Schwarz inequalities:

$$b \leq \sum_{k=0}^D \sum_{s \in \varpi(k,j)} N \|\mathbf{r}_{j-k}^s\|_G^2 + 2 \sum_{\substack{1 \leq k \leq D \\ 0 \leq q \leq D \\ 1 \leq K \leq k}} \sum_{\substack{s \in \varpi(k,j) \\ t \in \varpi(q,j-K)}} \|\mathbf{r}_{j-K-q}^t\|_G \|\mathbf{r}_{j-k}^s\|_G \tag{B.5}$$

The bounding from above is a classical consequence of the continuity of the fine problems.

$$\|\mathbf{r}_{j-k}^s\|_G^2 = \left\| \mathbf{A}^s \mathbf{J}^{sT} \left(\mathbf{s}^{s,F} (\mathbf{J}^s \mathbf{A}^{sT} \mathbf{S}^{G-1} (\mathbf{p}_{\Gamma,j-k} + \mathbf{b}^G); \mathbf{t}^{s,F}) - \mathbf{s}^{s,F} (\mathbf{J}^s \mathbf{A}^{sT} \mathbf{S}^{G-1} (\hat{\mathbf{p}}_{\Gamma} + \mathbf{b}^G); \mathbf{t}^{s,F}) \right) \right\|_G^2$$

$$\leq M^s \left| \mathbf{A}^{sT} \mathbf{S}^{G-1} \mathbf{e}_{j-k} \right|_{\mathbf{S}^s, G}^2 \leq M^s \|\mathbf{e}_{j-k}\|_G^2, \tag{B.6}$$

where we used that $\forall s, \mathbf{S}^G = \sum_{l=0}^N \mathbf{A}^l \mathbf{S}^{l,G} \mathbf{A}^{lT} \geq \mathbf{A}^s \mathbf{S}^s \mathbf{G} \mathbf{A}^{sT}$ in the SPD-matrix ordering. In the end, we have:

$$b \leq N \sum_{k=0}^D \sum_{s \in \varpi(k,j)} M^s \left\| \mathbf{e}_{j-k} \right\|_G^2 + 2 \sum_{\substack{1 \leq k \leq D \\ 0 \leq q \leq D \\ 1 \leq k \leq k}} \sum_{\substack{s \in \varpi(k,j) \\ i \in \varpi(q,j-k)}} \sqrt{M^s M^i} \left\| \mathbf{e}_{j-k-q} \right\|_G \left\| \mathbf{e}_{j-k} \right\|_G \tag{B.7}$$

Regarding the first degree term, the bounding from below is a consequence of the monotonicity:

$$\begin{aligned} a &= \sum_{k=0}^D \sum_{s \in \varpi(k,j)} \left((\mathbf{p}_{\Gamma j-k} + \mathbf{b}^G) - (\hat{\mathbf{p}}_{\Gamma} + \mathbf{b}^G) \right)^T \mathbf{S}^{G^{-1}} \mathbf{A}^s \mathbf{J}^{sT} \\ &\quad \left(\mathbf{s}^{s,F} (\mathbf{J}^s \mathbf{A}^s \mathbf{S}^{G^{-1}} (\mathbf{p}_{\Gamma j-k} + \mathbf{b}^G); \mathbf{f}^{s,F}) - \mathbf{s}^{s,F} (\mathbf{J}^s \mathbf{A}^s \mathbf{S}^{G^{-1}} (\hat{\mathbf{p}}_{\Gamma} + \mathbf{b}^G); \mathbf{f}^{s,F}) \right) \\ &\geq \sum_{k=0}^D \sum_{s \in \varpi(k,j)} \gamma^s \left| \mathbf{A}^{sT} \mathbf{S}^{G^{-1}} \mathbf{e}_{j-k} \right|_{\mathbf{S}^s, G}^2. \end{aligned} \tag{B.8}$$

References

- [1] O. Bettinotti, S. Guinard, E. Véron, P. Gosselet, On the implementation in Abaqus of the global-local iterative coupling and acceleration techniques, *Finite Elem. Anal. Des.* 236 (2024) 104152.
- [2] L. Gendre, O. Allix, P. Gosselet, F. Comte, Non-intrusive and exact global/local techniques for structural problems with local plasticity, *Comput. Mech.* 44 (2) (2009) 233–245.
- [3] M. Duval, J.-C. Passieux, M. Salaün, S. Guinard, Non-intrusive coupling: Recent advances and scalable nonlinear domain decomposition, *Arch. Comput. Methods Eng.* (2014) 1–22.
- [4] O. Bettinotti, O. Allix, B. Malherbe, A coupling strategy for adaptive local refinement in space and time with a fixed global model in explicit dynamics, *Comput. Mech.* (2013) 1–14.
- [5] G. Guguin, O. Allix, P. Gosselet, S. Guinard, On the computation of plate assemblies using realistic 3D joint model: A non-intrusive approach, *Adv. Model. Simul. Eng. Sci.* 3 (16) (2016) <http://dx.doi.org/10.1186/s40323-016-0069-5>.
- [6] A. Nouy, F. Pled, A multiscale method for semi-linear elliptic equations with localized uncertainties and non-linearities, *ESAIM: Math. Model. Numer. Anal.* 39 (2018).
- [7] M. Blanchard, O. Allix, P. Gosselet, G. Desmeure, Space/time global/local noninvasive coupling strategy: Application to viscoplastic structures, *Finite Elem. Anal. Des.* 156 (2019) 1–12.
- [8] M. Akterskaia, E. Jansen, S.R. Hallett, P. Weaver, R. Rolfes, Analysis of skin-stringer debonding in composite panels through a two-way global-local method, *Compos. Struct.* 202 (2018) 1280–1294.
- [9] T. Gerasimov, N. Noii, O. Allix, L. De Lorenzis, Non-intrusive global/local approach applied to phase-field modeling of brittle fracture, *Adv. Model. Simul. Eng. Sci.* 5 (14) (2018) <http://dx.doi.org/10.1186/s40323-018-0105-8>.
- [10] F. Aldakheel, N. Noii, T. Wick, P. Wriggers, A global-local approach for hydraulic phase-field fracture in poroelastic media, *Comput. Math. Appl.* 91 (2021) 99–121.
- [11] P. Gosselet, M. Blanchard, O. Allix, G. Guguin, Non-invasive global-local coupling as a Schwarz domain decomposition method: Acceleration and generalization, *Adv. Model. Simul. Eng. Sci.* 5 (4) (2018) <http://dx.doi.org/10.1186/s40323-018-0097-4>.
- [12] A. El Kerim, P. Gosselet, F. Magoulès, Asynchronous global-local non-invasive coupling for linear elliptic problems, *Comput. Methods Appl. Mech. Engrg.* 406 (2023) 115910, <http://dx.doi.org/10.1016/j.cma.2023.115910>.
- [13] C. Negrello, P. Gosselet, C. Rey, J. Pebral, Substructured formulations of nonlinear structure problems — influence of the interface condition, *Internat. J. Numer. Methods Engrg.* 107 (13) (2016) 1083–1105, <http://dx.doi.org/10.1002/nme.5195>.
- [14] A. Klawonn, M. Lanser, O. Rheinbach, Nonlinear FETI-DP and BDDC methods, *SIAM J. Sci. Comput.* 36 (2) (2014) A737–A765.
- [15] J.C. Miellou, D.E. Baz, P. Spiteri, A new class of asynchronous iterative algorithms with order intervals, *Math. Comp.* 67 (221) (1998) 237–255.
- [16] P. Spiteri, J.C. Miellou, D.E. Baz, Parallel asynchronous Schwarz and multisplitting methods for a nonlinear diffusion problem, *Numer. Algorithms* 33 (2003) 461–474.
- [17] P. Spiteri, J.-C. Miellou, D. Baz, Asynchronous Schwarz alternating methods with flexible communication for the obstacle problem, *Calculateurs parallèles, réseaux et systèmes répartis* 13 (2001) 47–66.
- [18] J. Bahi, J. Miellou, K. Rhoifir, Asynchronous multisplitting methods for nonlinear fixed point problems, *Numer. Algorithms* 15 (1997) 315–345.
- [19] A. Frommer, H. Schwandt, D.B. Szyld, Asynchronous weighted additive Schwarz methods, *Electron. Trans. Numer. Anal.* 5 (48–61) (1997) 1–5.
- [20] M. Chau, T. Garcia, P. Spiteri, Asynchronous Schwarz methods applied to constrained mechanical structures in grid environment, *Adv. Eng. Softw.* 74 (2014) 1–15.
- [21] E.K. Laitinen, A. Lapin, J. Pieskä, Asynchronous domain decomposition methods for continuous casting problem, *J. Comput. Appl. Math.* 154 (2003) 393–413.
- [22] X.-C. Tai, P. Tseng, Convergence rate analysis of an asynchronous space decomposition method for convex minimization, *Math. Comp.* 71 (239) (2002) 1105–1135.
- [23] C. Glusa, E. Boman, E. Chow, S. Rajamanickam, D. Szyld, Scalable asynchronous domain decomposition solvers, *SIAM J. Sci. Comput.* 42 (6) (2020) 384–409.
- [24] F. Magoulès, C. Venet, Asynchronous iterative sub-structuring methods, *Math. Comput. Simulation* 145 (2018) 34–49.
- [25] G. Gbikpi-Benissan, F. Magoulès, Asynchronous substructuring method with alternating local and global iterations, *J. Comput. Appl. Math.* 393 (2021) 116–133.
- [26] G. Gbikpi-Benissan, M. Rynkovskaya, F. Magoulès, Scalable asynchronous domain decomposition solvers for non-homogeneous elastic structures, *Adv. Eng. Softw.* 174 (2022) 103299.
- [27] F. Magoulès, D. Szyld, C. Venet, Asynchronous optimized Schwarz methods with and without overlap, *Numer. Math.* 137 (2017) 199–227.
- [28] J.C. Garay, F. Magoulès, D.B. Szyld, Synchronous and asynchronous optimized Schwarz methods for Poisson's equation in rectangular domains, *ETNA - Electron. Trans. Numer. Anal.* 55 (2022) 744–791.
- [29] M.E. Haddad, J.C. Garay, F. Magoulès, D.B. Szyld, Synchronous and asynchronous optimized Schwarz methods for one-way subdivision of bounded domains, *Numer. Lin. Alg. Appl.* 27 (2) (2020).

- [30] I. Yamazaki, E. Chow, A. Bouteiller, J. Dongarra, Performance of asynchronous optimized Schwarz with one-sided communication, *Parallel Comput.* 86 (2019) 66–81.
- [31] G. Gbikpi-Benissan, F. Magoulès, Resilient asynchronous primal schur method, *Appl. Math.* 67 (2022) 679–704.
- [32] J. Wolfson-Pou, E. Chow, Asynchronous multigrid methods, in: *IEEE International Parallel and Distributed Processing Symposium, IPDPS*, vol. 149, 2020.
- [33] J.C. Simo, R.L. Taylor, Consistent tangent operators for rate-independent elastoplasticity, *Comput. Methods Appl. Mech. Engrg.* 48 (1) (1985) 101–118, [http://dx.doi.org/10.1016/0045-7825\(85\)90070-2](http://dx.doi.org/10.1016/0045-7825(85)90070-2).
- [34] E.A. de Souza Neto, D. Perić, D.R.J. Owen, *Computational Methods for Plasticity*, John Wiley & Sons Ltd, 2008, <http://dx.doi.org/10.1002/9780470694626>.
- [35] J.-C. Passieux, J. Réthoré, A. Gravouil, M.-C. Baietto, Local/global non-intrusive crack propagation simulation using a multigrid X-Fem solver, *Comput. Mech.* 52 (6) (2013) 1381–1393.
- [36] O. Bettinotti, O. Allix, U. Perego, V. Oncea, B. Malherbe, Simulation of delamination under impact using a global local method in explicit dynamics, *Finite Elem. Anal. Des.* 125 (2017) 1–13, <http://dx.doi.org/10.1016/j.finel.2016.11.002>.
- [37] P. Spiteri, Parallel asynchronous algorithms: A survey, *Adv. Eng. Softw.* 149 (2020) 102896.
- [38] A. Hasanov, Integral convexity argument for plasticity function and monotonicity of iteration process for elasto-plastic problems, *Int. J. Non-Linear Mech.* 39 (2004) 1217–1226.
- [39] J. Mandel, Conditions de stabilité et postulat de drucker, in: *Rheology and Soil Mechanics*, International Union of Theoretical and Applied Mechanics, 1964, pp. 58–68, http://dx.doi.org/10.1007/978-3-642-46047-0_5.
- [40] A. Berman, R.J. Plemmons, *Nonnegative Matrices in the Mathematical Sciences*, SIAM, 1994.
- [41] E. Chow, A. Frommer, D.B. Szyld, Asynchronous Richardson iterations: Theory and practice, *Numer. Algorithms* 87 (4) (2021) 1635–1651.
- [42] L. Eisner, I. Koltracht, M. Neumann, Convergence of sequential and asynchronous nonlinear paracontractions, *Numer. Math.* 62 (1992) 305–319.
- [43] M. Pott, On the convergence of asynchronous iteration methods for nonlinear paracontractions and consistent linear systems, *Linear Algebra Appl.* 283 (1–3) (1998) 1–33.
- [44] L. Fang, P.J. Antsaklis, Asynchronous consensus protocols using nonlinear paracontractions theory, *IEEE Trans. Autom. Control* 53 (10) (2008) 2351–2355.
- [45] Y. Su, A. Bhaya, Convergence of pseudocontractions and applications to two-stage and asynchronous multisplitting for singular m-matrices, *SIAM J. Matrix Anal. Appl.* 22 (3) (2001) 948–964.
- [46] M.J. Gander, A.M. Stuart, Space-time continuous analysis of waveform relaxation for the heat equation, *SIAM J. Sci. Comput.* 19 (1998) 2014–2031.